Dynamical correlations in suspensions of charged rodlike macromolecules

Th. Kirchhoff[*]

Fakultät für Physik, Universität Konstanz, Postfach 5560, D-78434 Konstanz, Germany

H. Löwen[†]

Sektion Physik der Universität München, Theresienstraße 37, D-80333 München, Germany

R. Klein

Fakultät für Physik, Universität Konstanz, Postfach 5560, D-78434 Konstanz, Germany

Dynamical correlations of charged rodlike colloidal particles interacting via a Yukawa segment-segment potential are investigated using extensive Brownian dynamics computer simulations. The model and the parameters used in the simulations are particularly designed for aqueous suspensions of tobacco-mosaic viruses. Over a broad range of rod concentrations we calculate the translational long-time self-diffusion coefficient and study the orientational motion in the disordered phase. It is found that the relaxation of the orientational correlation has three different regimes: a diffusive short-time motion, another diffusive motion for intermediate times, and a *nondiffusive* long-time relaxation. Also dynamical correlations in the nematic phase and near the isotropic-nematic transition are calculated. The results are compared with experimental data.

PACS number(s): 36.30.Ey, 61.30.$-$v, 66.10.$-$x, 82.70.Dd

I. INTRODUCTION

Colloidal suspensions of rodlike viruses, such as the tobacco-mosaic virus (TMV) and bacterial fd virus, are convenient model systems for the study of anisotropic fluids. Liquid crystalline order was observed in TMV suspensions as early as 1936 [1] and experimental and theoretical work has continued to the present time [2,3]. These studies have been done on different levels: The first question concerns the nature of the effective interactions between the rodlike macromolecules. If the rods are sterically stabilized, an interaction model purely governed by excluded volume effects is appropriate, while for charged suspensions the bare Coulomb interrod repulsion is screened by the microscopic counterions, resulting in an effective segment-segment Yukawa interaction [4–7]. Next, based on a simple model with pairwise interactions between the rods, structural correlations in the disordered phase have been studied using liquid state theory or computer simulation [20,21]. The theoretical results can be compared to scattering experiments [8–10]; see, e.g., [11,12]. Third, there is an increasing amount of experimental data for the phase diagram of rods involving nematic, smectic, and fully crystalline phases, which is currently investigated also by theory and computer simulation [13].

While there is a growing understanding in these structural and thermodynamic questions, much less is known about *dynamical* correlations. It is fair to say that a purely microscopic theory of dynamical correlations is just beginning. The major problem one has for highly concentrated rod suspensions is that, unlike molecular liquid crystals, the short-time dynamics is not known due to the complexity of

solvent-mediated hydrodynamic interactions. For highly dilute but strongly interacting rods one may, however, safely neglect the many-body character of these interactions and the simple picture of Brownian dynamics is justified at least for highly charged rods at low concentration of added salt. Experimentally, more data have accumulated over the past decades: One may use birefringence methods, forced Rayleigh scattering, or dynamical light scattering to obtain information about the long-time decay of dynamical correlations.

Computer simulations with Brownian dynamics for a given interrod interaction provide a third powerful way to get direct insight into dynamical correlations since, apart from the statistical error, the results are exact. There are, however, only few computer simulations for rodlike suspensions. For infinitely thin uncharged needles, Doi *et al.* [14] have studied long-time self-diffusion. For a different phenomenological model of the rod interaction, Fixman [15] and subsequently Bitsanis *et al.* [16,17] have studied orientational long-time diffusion. Brownian dynamics simulations for the long-time translational and orientational self-diffusion for hard spherocylinders have been recently presented by Löwen [18].

However, for charged suspensions of the TMV or fd, a many-site Yukawa segment model is a much more realistic description of the interaction [4–7]. As far as we know there are no Brownian dynamics (BD) computer simulations for this model. The only exception is the recent work of Branka and Heyes [19], which is, however, confined to two sites, i.e., to moderately asymmetric rods. As we shall show, two sites are not sufficient in the intermediate and high concentration regimes for TMV and fd samples. Hence the two-site model is not appropriate for the experimentally relevant suspensions. Consequently, a full study with a many-segment model is necessary if one has a qualitative and quantitative comparison with the experimental data in mind.

In this paper we present extensive BD simulations for a Yukawa interaction model of five to nine sites, whose param-

[*]Electronic address: Thomas.Kirchhoff@uni-Konstanz.de

[†]Present address: Heinrich-Heine-Universität Düsseldorf, Institut für Theoretische Physik II, D-40225 Düsseldorf, Germany.

eters are adapted to a TMV suspension, over the whole concentration regime where the disordered phase is thermodynamically stable. In particular, translational and rotational long-time diffusion as well as the collective effective diffusion coefficient are studied as a function of rod concentration. We find qualitative agreement with experiments. Furthermore we show that the long-time orientational relaxation is not a standard diffusion process over the unit sphere. This is known for reversible Newtonian dynamics [22–24], relevant for rodlike molecules, but it was not yet recognized for irreversible Brownian dynamics in previous simulations [14,16].

We finally study the isotropic-nematic transition. After having located it we calculate the corresponding dynamical correlations. Due to a release of constraints on translational motion from interference of neighboring particles it is found that the translational long-time coeffcient increases if one passes through the isotropic-nematic transition.

The paper is organized as follows. In Sec. II, the model is described. The algorithm and details of the computer simulation are discussed in Secs. III and IV. Structural and dynamical correlations are defined in Sec. V and results are presented in Sec. VI. Finally, we conclude in Sec. VII.

II. MODEL

We consider an ensemble of N rods in a volume Ω. The cylindrical rods are monodisperse with a length L and a diameter d. For concrete calculations we chose TMV parameters $L = 300$ nm and $d = 18$ nm. Thermodynamically, the rod suspension is characterized by its number concentration $c = N/\Omega$ and the temperature T. The rod concentration c is conveniently measured in terms of the overlap concentration $c^* \equiv 1/L^3$. The temperature is taken to be fixed to room temperature $T = 298$ K. A typical rod configuration can be characterized by its center-of-mass coordinates $\{\mathbf{r}_i, i=1,\ldots,N\}$ and its orientations specified by unit vectors $\{\mathbf{u}_i, i=1,\ldots,N\}$.

The essential input of any statistical mechanics description are the interrod interactions. We rely on a simple but realistic picture of the interrod forces and torques. The screened electrostatic interaction among suspended rods is described by a Yukawa segment model [4–6,25]. In this model, the total rod charge Q is distributed equally among n segments located along the rod axis. The segments belonging to different rods interact through the repulsive part of the standard Derjaguin-Landau-Verwey-Overbeek (DLVO) potential, which is of Yukawa type. Since the interaction is assumed to be pairwise, the total potential energy in a given rod configuration is

$$U_{\text{tot}} = \sum_{i=1, j>i}^{N} U(\mathbf{r}_i - \mathbf{r}_j, \mathbf{u}_i, \mathbf{u}_j), \tag{1}$$

where the orientation-dependent interrod potential $U(\mathbf{r}_i - \mathbf{r}_j, \mathbf{u}_i, \mathbf{u}_j)$ is the sum of all segment-segment interactions

$$U(\mathbf{r}_i - \mathbf{r}_j, \mathbf{u}_i, \mathbf{u}_j) = \frac{(Q/n)^2}{4\pi\epsilon\epsilon_0} \sum_{\alpha,\beta=1}^{n} \frac{e^{-\kappa r_{\alpha\beta}^{ij}}}{r_{\alpha\beta}^{ij}}, \tag{2}$$

with the interrod segment distance

$$r_{\alpha\beta}^{ij} = |\mathbf{r}_i - \mathbf{r}_j + \mathbf{u}_i d_n (2\alpha - 1 - n)/2 - \mathbf{u}_j d_n (2\beta - 1 - n)/2|, \tag{3}$$

d_n denoting the distance between two neighboring segments along a rod

$$d_n = \frac{L}{\sqrt{(n+1)(n-1)}}. \tag{4}$$

This expression ensures that the quadrupolar moment of the segmented rod is that of a homogeneous line charge of length L. Furthermore, the Debye-Hückel screening constant κ is given by

$$\kappa^2 = \frac{cQe + \Sigma_i c_i q_i^2}{\epsilon\epsilon_0 k_B T}. \tag{5}$$

e is the elementary charge, cQ/e the concentration of counterions (assumed as single valenced), and c_i the concentration of additional salt ions with charges q_i. Finally, ϵ_0 is the dielectric constant and ϵ the relative dielectric constant of the solvent; we take henceforth $\epsilon = 78$ (water at room temperature).

Let us note three points concerning this Yukawa segment model. First, the static properties of the fd virus and the TMV suspensions as measured by dynamic light scattering experiments [8–11] could be reproduced well by Monte Carlo (MC) simulations [11], taking the total rod charge Q as one fit parameter.

Second, the general Yukawa form was recently justified in the framework of the ''primitive model,'' taking the counterions explicitly into account. Within *ab initio* calculations one of us (H.L.) [7] has shown that the Yukawa interaction is indeed a reasonable fit to the effective many-body forces and torques. However, the actual rod charge and the screening constant κ entering into the Yukawa description may significantly deviate from the DLVO predictions. A cylindrical Poisson-Boltzmann cell model, which also leads to an effective Yukawa-segment model, is more appropriate for highly interacting charged rods. This cell model can be analytically solved without added salt ions, while for added salt only a numerical solution is possible [26]. In the following we have fixed the parameter Q, thus empirically fitting the experimental structural data for a TMV suspension.

Third, since the rods cannot penetrate, one should also include a hard core in the interaction. However, for the rod concentrations used in this paper we never observed such a rod overlap during the simulation. Hence we can safely neglect the excluded volume part completely. It should be noted, however, that this also depends strongly on the number of sites n. If n is small, say, $n \approx 2 - 3$, then rods can cross in the high concentration regime. Therefore we again stress the necessity of a high site number n ($n>4$) for doing simulations for TMVs.

Next, the short-time dynamics of the rods has to be specified. As already mentioned, we neglect the solvent-mediated hydrodynamic interactions, which are due to the velocity field induced by the motion of all macroparticles. The justification in doing so is that we are dealing with highly diluted

systems (i.e., with low volume fraction of the rods), where the many-body effects of hydrodynamic interactions can be considered to be small. Hence only hydrodynamic one-particle properties are taken into account in describing the short-time self-diffusion coefficients $D_0^\perp$ and $D_0^\parallel$ [27]. These coefficients $D_0^\perp, D_0^\parallel$ have been calculated by Tirado *et al.* [28]:

$$D_0^\perp = \frac{D_0}{4\pi}(\ln p + 0.839 + 0.185/p + 0.233/p^2), \qquad (6)$$

$$D_0^\parallel = \frac{D_0}{2\pi}(\ln p - 0.207 + 0.980/p - 0.133/p^2), \qquad (7)$$

with $D_0 = k_B T/\eta_s L$ and the length-to-width ratio $p = L/d$. Here k_B is Boltzmann's constant and η_s is the shear viscosity of the solvent. The translational diffusion coefficient of the center-of-mass coordinate is given for a free rod by

$$D_0^T = \frac{1}{3}(D_0^\parallel + 2D_0^\perp). \qquad (8)$$

The short-time motion of the orientational degrees of freedom as embodied in the unit vectors $\{\mathbf{u}_i\}$ is described by isotropic Brownian motion on the unit sphere characterized by an orientational short-time self-diffusion coefficient D_0^R [27], which is given by [28]

$$D_0^R = \frac{3D_0}{\pi L^2}(\ln p - 0.662 + 0.917/p - 0.050/p^2). \qquad (9)$$

These diffusion coefficients define typical time scales. An orientational relaxation time can be defined through

$$\tau_0^R = \frac{1}{2D_0^R}. \qquad (10)$$

This is the time it takes a free rod to lose all memory about its initial orientation. Similarly, a translational relaxation time can be defined

$$\tau_0^T = \frac{L^2}{2D_0^T}. \qquad (11)$$

For the case of the TMV $\tau_0^R = 1.5$ ms and $\tau_0^T = 10$ ms.

III. BROWNIAN DYNAMICS ALGORITHM

For the simulation of the Brownian motion of rods we adopt an algorithm proposed by Ermak [29] for BD simulations of spheres that is readily generalized to rods [18]. In a BD simulation the trajectories $\{\mathbf{r}_i(t), \mathbf{u}_i(t)\}$ of the particles are generated by integrating the corresponding Langevin equations with a finite time step Δt. To obtain the corresponding finite-difference equations we split the center-of-mass position $\mathbf{r}_i(t)$ of rod i into a part parallel and a part perpendicular to the rod orientation $\mathbf{u}_i(t)$:

$$\mathbf{r}_i(t) = \mathbf{r}_i^\parallel(t) + \mathbf{r}_i^\perp(t), \qquad (12)$$

with $\mathbf{r}_i^\parallel(t)$ given by

$$\mathbf{r}_i^\parallel(t) \equiv [\mathbf{u}_i(t) \cdot \mathbf{r}_i(t)]\mathbf{u}_i(t). \qquad (13)$$

The same kind of separation can be done for the total force $\mathbf{F}_i(t)$ acting on the center of rod i due to the interactions with all other rods:

$$\mathbf{F}_i(t) = \mathbf{F}_i^\parallel(t) + \mathbf{F}_i^\perp(t). \qquad (14)$$

The update equation for $\mathbf{r}_i^\parallel(t)$ can be written as

$$\mathbf{r}_i^\parallel(t + \Delta t) = \mathbf{r}_i^\parallel(t) + \frac{\Delta t}{k_B T}D_0^\parallel \mathbf{F}_i^\parallel(t) + (\Delta r^\parallel)\mathbf{u}_i(t). \qquad (15)$$

Here $(\Delta r^\parallel)$ denotes a Gaussian random displacement with zero mean and variance $\langle(\Delta \mathbf{r}^\parallel)^2\rangle_G = 2D_0^\parallel \Delta t$, $\langle\rangle_G$ denoting the average over the Gaussian distribution. The perpendicular part $\mathbf{r}_i^\perp(t)$ has an analogous update equation

$$\mathbf{r}_i^\perp(t + \Delta t) = \mathbf{r}_i^\perp(t) + \frac{\Delta t}{k_B T}D_0^\perp \mathbf{F}_i^\perp(t) + (\Delta r_1^\perp)\mathbf{e}_{i1}(t)$$
$$+ (\Delta r_2^\perp)\mathbf{e}_{i2}(t). \qquad (16)$$

The random displacements $(\Delta r_1^\perp)$ and $(\Delta r_2^\perp)$ are uncorrelated Gaussian random numbers with zero mean and variance $2D_0^\perp \Delta t$. Here the vectors $\mathbf{e}_{i1}(t)$ and $\mathbf{e}_{i2}(t)$ are two orthogonal unit vectors, which are both perpendicular to $\mathbf{u}_i(t)$.

Note that both update equations can be compactly summarized as

$$\mathbf{r}_i(t + \Delta t) = \mathbf{r}_i(t) + \frac{\Delta t}{k_B T}\mathbf{D}_i^T \mathbf{F}_i(t) + \Delta \mathbf{r}_i, \qquad (17)$$

with the diffusion tensor

$$\mathbf{D}_i^T = D_0^\perp(\mathbf{1} - \mathbf{u}_i\mathbf{u}_i) + 2D_0^\parallel \mathbf{u}_i\mathbf{u}_i, \qquad (18)$$

$\mathbf{u}_i\mathbf{u}_i$ representing the dyadic product of $\mathbf{u}_i$ and the variance-covariance matrix given by

$$\langle(\Delta r_{i\alpha})(\Delta r_{i\beta})\rangle = 2D_{i\alpha\beta}^T \Delta t. \qquad (19)$$

Here $\Delta \mathbf{r}_i$ follows has a multivariate Gaussian distribution. This equation is independent of the coordinate system used, whereas for computational purposes it is more convenient to use the above form (15) and (16) of the update equation, where the diffusion tensor $\mathbf{D}^T$ is evaluated in the principal frame of reference in which it becomes diagonal.

Finally, the orientational update equation for $\mathbf{u}_i(t)$ is

$$\mathbf{u}_i(t + \Delta t) = \mathbf{u}_i(t) + \frac{\Delta t}{k_B T}D_0^R \mathbf{M}_i(t)\mathbf{u}_i(t) + x_1\mathbf{e}_{i1}(t) + x_2\mathbf{e}_{i2}(t), \qquad (20)$$

with $\mathbf{M}_i(t)$ denoting the total center-of-mass torque acting on rod i and x_1, x_2 being two uncorrelated Gaussian random numbers with zero mean and variance $2D_0^R \Delta t$. After application of Eq. (20), $\mathbf{u}_i(t + \Delta t)$ has to be renormalized such that $|\mathbf{u}_i(t + \Delta t)| = 1$. The coupling of rotation and translation happens through the orientation-dependence of $\mathbf{D}^T(t)$. Obviously, for $D_0^\parallel = D_0^\perp$, rotation and translation become completely decoupled.

The BD algorithm presented up to now is exact to order Δt, its error is of $O(\Delta t^2)$. It can easily be modified such that the error introduced in each time step is of $O(\Delta t^3)$ [30–32]. For the translational part, we obtain via Eq. (17) a first-order estimate of the position denoted by $\mathbf{r}_i'(t+\Delta t)$. Then the time step is repeated using the mean of the forces at positions $\mathbf{r}_i(t)$ and $\mathbf{r}_i'(t+\Delta t)$. We thus have

$$\mathbf{r}_i(t+\Delta t) = \mathbf{r}_i(t) + \frac{\Delta t}{k_B T} \left\{ \frac{1}{2} [\mathbf{D}_i^T(t)\mathbf{F}_i(t) \right.$$
$$\left. + \mathbf{D}_i'^T(t+\Delta t)\mathbf{F}_i'(t+\Delta t)] \right\} + \Delta \mathbf{r}_i, \quad (21)$$

where

$$\langle (\Delta r_{i\alpha})(\Delta r_{i\beta}) \rangle = 2 \left\{ \frac{1}{2} [D_{i\alpha\beta}^T(T) + D_{i\alpha\beta}'^T(t+\Delta t)] \right\} \Delta t, \tag{22}$$

written in the compact notation of Eq. (17). The orientational second-order update equation is

$$\mathbf{u}_i(t+\Delta t) = \mathbf{u}_i(t) + \frac{\Delta t}{k_B T} D_0^R \left\{ \frac{1}{2} [\mathbf{M}_i(t)\mathbf{u}_i(t) + \mathbf{M}_i'(t+\Delta t) \right.$$
$$\left. \times \mathbf{u}_i'(t+\Delta t)] \right\} + \Delta \mathbf{u}_i, \tag{23}$$

where

$$\Delta \mathbf{u}_i = 2 \left\{ \frac{1}{2} [x_1 \mathbf{e}(t)_{i1} + x_2 \mathbf{e}_{i2}(t) + x_1' \mathbf{e}_{i1}(t+\Delta t) \right.$$
$$\left. + x_2' \mathbf{e}_{i2}(t+\Delta t)] \right\}. \tag{24}$$

We have used this algorithm, which requires a doubled CPU time per step as compared to the first-order algorithm, since the systematic error is smaller. It was carefully checked that the time step was small enough by doing runs with different time steps and comparing the results. It was also checked that static pair correlation data are in perfect agreement with Monte Carlo results.

IV. SIMULATION

Most runs were performed using $N=512$ rods with $n=5$ segments. For comparison with former MC results we used $N=256$ rods and $n=3$ segments. For concentrations $c>8c^*$ even 5 segments are not sufficient, especially in the vicinity of the isotropic-nematic transition, which occurs around $15c^*$. For these high concentrations 9 segments were used. Standard periodic boundary conditions with a cubic simulation box of length L_b were applied. All parameters were chosen to resemble a TMV suspension. In particular, the rod charge of $Q=390e$ taken from a comparison of experimental data and MC simulations for static pair correlations [11] seems to be a reasonable choice for all densities considered here $(0.01c^* - 24c^*)$.

As a starting configuration we used an ordered configuration with the centers of the rods placed on fcc lattice positions and the rod axes all pointing into the same direction. To decide when thermal equilibrium was reached we monitored the translational order parameter

$$\rho(\mathbf{k}) = \frac{1}{N} \sum_{i=1}^N \cos(\mathbf{k} \cdot \mathbf{r}_i), \tag{25}$$

where $\mathbf{r}_i$ is the vector of the center of mass of the ith rod and $\mathbf{k} = [(2N)^{1/3}\pi/L_b](-1,1,-1)$ is a reciprocal lattice vector of the initial lattice.

To detect rotational order we monitor the quantity

$$P_1(t) = \frac{1}{N} \sum_{i=1}^N P_1(\mathbf{u}_i(0) \cdot \mathbf{u}_i(t)), \tag{26}$$

where $P_1(x) = x$ is the first Legendre polynomial [33]. In the disordered (fluid) phase, $\rho(\mathbf{k})$ and $P_1(t)$ start out at 1 and finally fluctuate around zero, at which point we start to take ensemble averages. We have also monitored the nematic order parameter as given by Allen *et al.* [34]. The nematic order parameter is given through the largest eigenvalue λ_+ of the $\mathbf{Q}$ tensor

$$\mathbf{Q} = \frac{1}{N} \sum_{i=1}^N \left(\frac{3}{2} \mathbf{u}_i \mathbf{u}_i - \frac{1}{2} \mathbf{1} \right). \tag{27}$$

$\mathbf{u}_i \mathbf{u}_i$ denotes the dyadic product of the orientation vectors of particle i.

The equilibration phase takes about 100 000 steps, depending upon density. For production runs we used a time step of $\Delta t = 0.000\,64\tau_0^R$. For densities $c>8c^*$, Δt was taken as $0.000\,32\tau_0^R$. The number of time steps used for taking statistics was between 1.4×10^6 at $0.1c^*$ to 0.6×10^6 at $18c^*$.

V. CORRELATION FUNCTIONS

A. Static correlation functions

The main static correlation functions are the structure factor and the pair distribution function. In the case of rods they are related by a Hankel transform [4,6]. The pair distribution function is defined via

$$g(\mathbf{r}_1 - \mathbf{r}_2, \mathbf{u}_1, \mathbf{u}_2) = \left\langle \sum_{i,j=1; i\neq j}^N \delta(\mathbf{r}_i - \mathbf{r}_1)\delta(\mathbf{r}_j - \mathbf{r}_2) \right.$$
$$\left. \times \delta(\mathbf{u}_i - \mathbf{u}_1)\delta(\mathbf{u}_j - \mathbf{u}_2) \right\rangle, \tag{28}$$

where $\langle\rangle$ is a canonical average. It can be expanded [5] in the space fixed coordinate frame as

$$g(\mathbf{r}, \mathbf{u}_1, \mathbf{u}_2) = \sum_{\ell_1, \ell_2, \ell} g_{\ell_1 \ell_2 \ell}(r) \Phi_{\ell_1 \ell_2 \ell}(\mathbf{u}_1, \mathbf{u}_2, \hat{\mathbf{r}}), \quad \hat{\mathbf{r}} = \frac{\mathbf{r}}{r}, \tag{29}$$

where the angular part can be decomposed into spherical harmonics

$$\Phi_{\ell_1 \ell_2 \ell} = \sum_{m_1,m_2,m} C(\ell_1 \ell_2 \ell; m_1 m_2 m) Y_{\ell_1 m_1}$$
$$\times (\mathbf{u}_1) Y_{\ell_2 m_2}(\mathbf{u}_2) Y_{\ell m}(\hat{\mathbf{r}}). \qquad (30)$$

Here $C(\ell_1 \ell_2 \ell; m_1 m_2 m)$ is a Clebsch-Gordan coefficient and $Y_{\ell m}(\mathbf{u})$ a spherical harmonic. The physical meaning of the first few coefficents in Eq. (29) is the following: The function

$$g_{cc}(r) \equiv \langle g(\mathbf{r}, \mathbf{u}_1, \mathbf{u}_2) \rangle_{\mathbf{u}_1 \mathbf{u}_2} = (4\pi)^{-3/2} g_{000}(r) \qquad (31)$$

is the usual center-center distribution function, r being the distance between the centers of mass of two rods. The average $\langle \rangle_{\mathbf{u}_1 \mathbf{u}_2}$ is defined as the unweighted average over all directions

$$\langle \rangle_{\mathbf{u}_1 \mathbf{u}_2} \equiv \frac{1}{(4\pi)^2} \int d\mathbf{u}_1 d\mathbf{u}_2 \cdots . \qquad (32)$$

The angular correlations can be described through the expression

$$g_{P_2}(r) \equiv \frac{\langle g(\mathbf{r}, \mathbf{u}_1, \mathbf{u}_2) P_2(\cos\theta_{12}) \rangle_{\mathbf{u}_1 \mathbf{u}_2}}{\langle g(\mathbf{r}, \mathbf{u}_1, \mathbf{u}_2) \rangle_{\mathbf{u}_1 \mathbf{u}_2}} = \frac{1}{\sqrt{5}} \frac{g_{220}(r)}{g_{000}(r)}. \qquad (33)$$

Here $P_2(x) = (3x^2 - 1)/2$ denotes the second Legendre polynomial and θ_{12} is the angle between $\mathbf{u}_1$ and $\mathbf{u}_2$. The function $g_{P_2}(r)$ is positive when rods tend to stay parallel, whereas it is negative if two rods with center-of-mass distance r are on average perpendicular. For a fully aligned parallel configuration we have $g_{P_2}(r) \equiv 1$, while for a perpendicular arrangement $g_{P_2}(r) \equiv -1/2$. For completely uncorrelated configurations $g_{P_2}(r) \equiv 0$.

Similarly, the coefficient $g_{202}(r)$ has a negative value if on average the connection vector $\hat{\mathbf{r}}$ of the center of mass of two rods is perpendicular to the orientation vector $\mathbf{u}$ of one of the rods. $g_{202}(r)$ is positive if $\hat{\mathbf{r}}$ and $\mathbf{u}$ are parallel on average. For completely uncorrelated configurations $g_{202}(r) \equiv 0$.

The static structure factor $S(k)$ can directly be measured in laser light scattering experiments. It is defined by [6]

$$S(k) = \frac{1}{F(k)N} \left\langle \sum_{i,j=1}^{N} e^{i\mathbf{k} \cdot (\mathbf{r}_i - \mathbf{r}_j)} \right.$$
$$\left. \times \frac{\sin(\mathbf{k} \cdot \mathbf{u}_i L/2)}{\mathbf{k} \cdot \mathbf{u}_i L/2} \frac{\sin(\mathbf{k} \cdot \mathbf{u}_j L/2)}{\mathbf{k} \cdot \mathbf{u}_j L/2} \right\rangle. \qquad (34)$$

The function $F(k)$ is the form factor of a rod; it depends only on the shape of the particles and is given by

$$F(k) = \left\langle \left(\frac{\sin(\mathbf{k} \cdot \mathbf{u}_i L/2)}{\mathbf{k} \cdot \mathbf{u}_i L/2} \right)^2 \right\rangle, \qquad (35)$$

which can be written as [35]

$$F(k) = \left(\frac{2}{kL} \int_0^{kL/2} dx j_0(x) \right) - [j_0(kL/2)]^2, \qquad (36)$$

with $j_0(x)$ being the first spherical Bessel function.

B. Dynamical translational correlation functions

As regards dynamical correlations, we concentrate mainly on single-particle properties considering the autocorrelation functions

$$W^T(t) = \frac{1}{N} \sum_{i=1}^{N} \frac{\langle [\Delta \mathbf{r}_i(t)]^2 \rangle}{6} \equiv D^T(t)t, \qquad (37)$$

$$W^{\parallel}(t) = \frac{1}{N} \sum_{i=1}^{N} \frac{\langle [\Delta \mathbf{r}_i^{\parallel}(t)]^2 \rangle}{2} \equiv D^{\parallel}(t)t, \qquad (38)$$

$$W^{\perp}(t) = \frac{1}{N} \sum_{i=1}^{N} \frac{\langle [\Delta \mathbf{r}_i^{\perp}(t)]^2 \rangle}{4} \equiv D^{\perp}(t)t, \qquad (39)$$

with

$$\Delta \mathbf{r}_i(t) = \mathbf{r}_i(0) - \mathbf{r}_i(t), \qquad (40)$$

$$\Delta \mathbf{r}_i^{\parallel}(t) = [\Delta \mathbf{r}_i(t) \cdot \mathbf{u}_i(0)] \mathbf{u}_i(0), \qquad (41)$$

$$\Delta \mathbf{r}_i^{\perp}(t) = \Delta \mathbf{r}_i(t) - \Delta \mathbf{r}_i^{\parallel}(t). \qquad (42)$$

By these equations we have defined time-dependent diffusion coefficients $D^T(t)$, $D^{\parallel}(t)$, and $D^{\perp}(t)$. The function $W^T(t)$ is the ordinary mean-square displacement of the center-of-mass coordinate for a single rod, averaged over an ensemble of trajectories. From the slope of this function we obtain the long-time limit of the translational self-diffusion coefficient D_L^T,

$$D_L^T \equiv \lim_{t \to \infty} \frac{W^T(t)}{t} = \lim_{t \to \infty} \frac{dW^T(t)}{dt}. \qquad (43)$$

The quantities $W^{\parallel}(t)$ and $W^{\perp}(t)$ measure the displacement of the center-of-mass coordinate relative to the orientation that the rod had at time $t=0$. It is expected that the memory about the initial orientation is lost after some time such that the slopes of $W^{\parallel}(t)$ and $W^{\perp}(t)$ become the same and equal to the slope of $W^T(t)$.

C. Dynamical orientational correlation functions

The orientational dynamics of an ensemble of *non-interacting* rods can be cast into a diffusion equation on the unit sphere for the conditional probability density $P(\mathbf{u}_0, \mathbf{u}; t)$ to have orientation $\mathbf{u}$ at time t when at $t=0$ the orientation was $\mathbf{u}_0$. If we choose $\mathbf{u}_0 = (0,0,1)$ and θ and ϕ to be the azimuthal and polar angles of the unit vector $\mathbf{u} = (\sin\theta \cos\phi, \sin\theta \sin\phi, \cos\theta)$, then this Debye rotational diffusion equation [36] reads

$$\frac{\partial P(\mathbf{u}_0, \mathbf{u}; t)}{\partial t} = D_0^R \left[\frac{1}{\sin\theta} \frac{\partial}{\partial \theta} \left(\sin\theta \frac{\partial P}{\partial \theta} \right) + \frac{1}{\sin^2\theta} \frac{\partial^2 P}{\partial \phi^2} \right], \qquad (44)$$

where D_0^R is the short-time orientational diffusion coefficient. Hence the orientation vector $\mathbf{u}(t)$ performs a random walk on the unit sphere. The solution of this diffusion equation can be expanded in terms of Legendre polynomials $P_\ell(x)$,

$$P(\mathbf{u}_0, \mathbf{u}; t) = \sum_{\ell=1}^{\infty} \left(\frac{2\ell+1}{4\pi} \right) P_\ell(\mathbf{u}(0) \cdot \mathbf{u}(t)) e^{-D_0^R \ell(\ell+1)t},$$

(45)

resulting in the orientational correlation functions

$$\langle P_\ell(\mathbf{u}(0) \cdot \mathbf{u}(t)) \rangle = e^{-D_0^R \ell(\ell+1)t}.$$

(46)

In the case of an *interacting* system we define the rotational correlation function $W_\ell(t)$ and a set of corresponding time-dependent orientational diffusion coefficients as

$$W_\ell(t) = \langle P_\ell(\mathbf{u}(0) \cdot \mathbf{u}(t)) \rangle \equiv e^{-D_\ell^R(t)\ell(\ell+1)t}.$$

(47)

If $D_\ell^R(t)$ becomes independent of t and ℓ for long times, the orientational long-time motion is diffusive on the unit sphere with an orientational long-time self-diffusion coefficient D_L^R defined as

$$D_L^R \equiv -\lim_{t \to \infty} \frac{1}{\ell(\ell+1)} \ln W_\ell(t) \quad \text{for all } \ell.$$

(48)

In particular, this is valid for noninteracting rods where $D_L^R = D_0^R$. On the other hand, if the long-time behavior of $D_\ell^R(t)$ depends on ℓ, the motion does *not* correspond to standard diffusion on the unit sphere. Then the two basic assumptions of Debye theory, namely, uncorrelated and small jumps in orientation space, are not fulfilled. For more details, we refer to the extensive discussion in Ref. [16].

D. Collective dynamical correlation functions

The dynamic structure factor of a solution of interacting Brownian particles can be directly measured through dynamical light scattering experiments. For rodlike particles, $S(k,t)$ can be written as [6,27]

$$S(k,t) = \frac{1}{NF(k)} \left\langle \sum_{i,j=1}^{N} e^{i\mathbf{k} \cdot [\mathbf{r}_i(0) - \mathbf{r}_j(t)]} \right.$$

$$\left. \times \frac{\sin[\mathbf{k} \cdot \mathbf{u}_i(0)L/2]}{\mathbf{k} \cdot \mathbf{u}_i(0)L/2} \frac{\sin[\mathbf{k} \cdot \mathbf{u}_j(t)L/2]}{\mathbf{k} \cdot \mathbf{u}_j(t)L/2} \right\rangle. \quad (49)$$

From $S(k,t)$ one can define an effective short-time collective diffusion coefficient

$$D_{\text{eff}}(k) = \frac{\Gamma_1(k)}{k^2} = -\frac{1}{k^2} \left. \frac{\partial \ln S(k,t)}{\partial t} \right|_{t=0}, \quad (50)$$

$\Gamma_1(k)$ denoting the first cumulant of the dynamic structure factor. If hydrodynamic interactions are neglected (as we did in our model) it can be shown [21] that the first cumulant of an interacting system, $\Gamma_{1,\text{int}}(k)$, is related to the first cumulant for the corresponding noninteracting system, $\Gamma_{1,0}(k)$, and to the static structure factor $S(k)$ of the interacting system:

$$\Gamma_{1,\text{int}}(k) = \frac{1}{S(k)} \Gamma_{1,0}(k). \quad (51)$$

For anisotropic translational diffusion $\Gamma_{1,0}(k)$ is given analytically by [21]

$$\Gamma_{1,0}(k) = \sum_{\substack{\ell=0 \\ \ell \text{ even}}}^{\infty} \left\{ [\ell(\ell+1)D_0^R + D_0^\perp k^2] a_\ell^2 \right.$$

$$\left. + (D_0^\| - D_0^\perp)k^2(2\ell+3) \left(\frac{j_{\ell+1}(kL/2)}{kL/2} \right)^2 \right\},$$

(52)

where the coefficients $a_\ell(kL)$ are given by integrals over spherical Bessel functions $j_\ell(x)$,

$$a_\ell(kL) = \begin{cases} 0 & \text{for } \ell \text{ odd} \\ i^\ell \sqrt{2\ell+1} \dfrac{2}{kL} \displaystyle\int_0^{kL/2} dx\, j_\ell(x) & \text{for } \ell \text{ even}. \end{cases}$$

(53)

At this stage two points can be concluded. First, one can calculate the static structure factor using two routes: either using the initial slope of the dynamical structure factor or implementing its static definition given by Eq. (34). A comparison of the results obtained by these different routes may be used as a consistency check of the simulation. Second, by comparing the first cumulant to experimental data, one can get hints about the importance of hydrodynamic interactions among suspended rodlike particles.

VI. RESULTS

A. Static correlations

First we have calculated different coefficients of the pair correlation function, namely, $g_{cc}(r)$, $g_{202}(r)$, and $g_{P_2}(r)$, defined in Sec. V A. The results are shown in Fig. 1. In order to check the program we have also tested them against previously published MC data [11,21]. Figure 1(a) gives data for the density regions of $0.28c^*$ up to $1.4c^*$. Figure 1(b) extends the comparison to higher concentrations, where $5.6c^*$ represents the upper limit of the concentration regime, which has been simulated with the MC program. As it should be, the results coincide. We note that the positions of the first peaks in $g_{cc}(r)$, $g_{202}(r)$, and $g_{P_2}(r)$ coincide for the highest concentration ($5.6c^*$). This fact was previously unnoticed and its interpretation is that at higher concentration neighboring rods tend to stay parallel, whereas at rather low concentrations neighboring particles tend to orient perpendicularly, which is energetically more favorable.

In order to fix the number of segments necessary to simulate even higher concentrations we compared the static output of three BD runs with $n = 3$, 5, and 7 segments in Fig. 2. It can be seen that $n = 3$ segments are clearly not enough to simulate our rod suspension at such high densities as $8c^*$, but 5 segment results are indistinguishable from the results obtained from 7 segment runs. We therefore use 5 segments in our dynamical simulations for densities up to $8c^*$. For $c > 8c^*$ the situation becomes more difficult. We found that
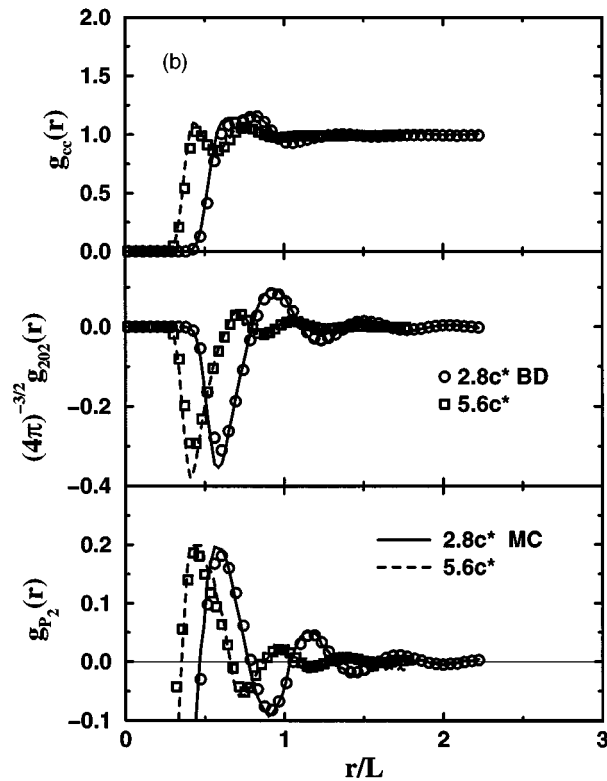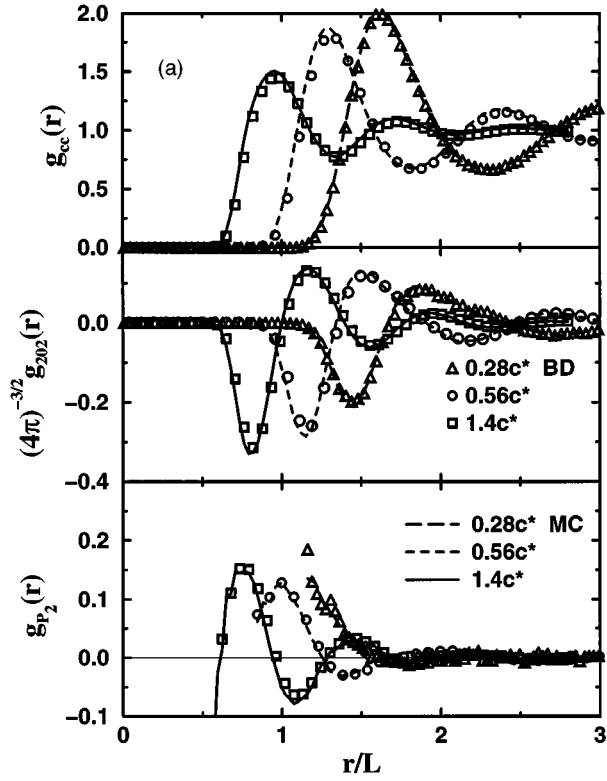
FIG. 1. Comparison of BD and MC pair distribution functions. Shown are the coefficients $g_{cc}(r)$, $(4\pi)^{-3/2}g_{202}(r)$, and $g_{P_2}(r)$. The symbols denote BD data, the lines MC data. The system parameters are as follows: $N=256$ rods, $n=3$ segments, $Q=390e$, $L=300$ nm, and $d=18$ nm. (a) Low and intermediate concentration regimes, $c=0.28c^*$, $0.56c^*$, and $1.4c^*$. (b) High concentration regime $c=2.8c^*$ and $5.6c^*$.
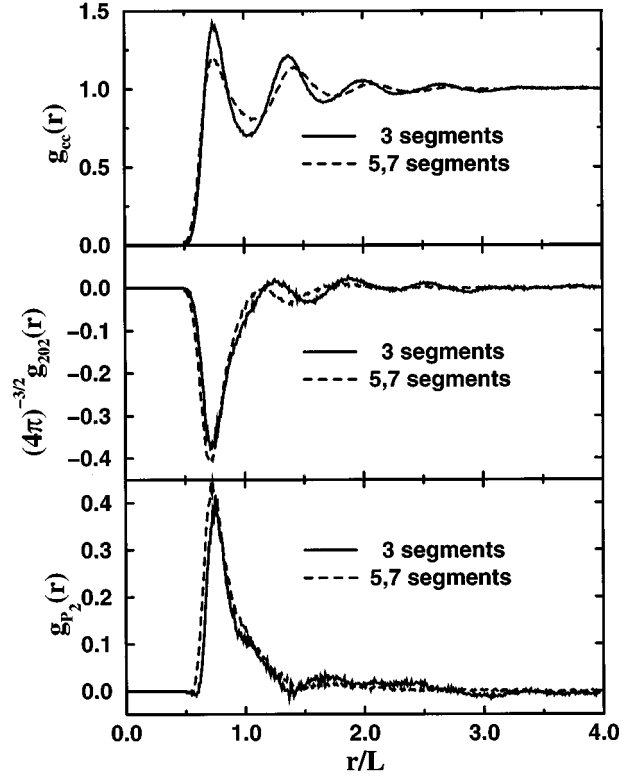

FIG. 2. Comparison of pair distribution function coefficients for different segment numbers $n=3$, 5, and 7 at a density of $c=8c^*$. Data for 7 segments are indistinguishable from those for 5 segments.

if we use 9 segments the system undergoes an isotropic-nematic phase transition at a concentration between $14c^*$ and $16c^*$. This is shown in Fig. 3(a). The nematic order parameter λ_+ is monitored for about $400\tau_0^R$. At $c>14c^*$ it does not decay any more but fluctuates around some fixed positive value. This transition cannot be observed with fewer than 9 segments. For the concentration regime between $8c^*$ and $24c^*$ we therefore used 9 segments. We checked that with 11 segments the results are within the same statistical error as with 9 segments.

Hence an isotropic-nematic phase transition is observed for rodlike particles interacting through a Yukawa potential. To create more evidence to support this fact than just showing nondecaying order parameter curves, we conducted the following experiment: At $c=18c^*$ and with a concentration of 0.05 mmol of monovalent salt, we equilibrate the system until the nematic order parameter settles around a constant value of about 0.6. Note that this arises because the weaker interrod interaction lowers the value of the nematic order parameter compared to its value without salt. Then we remove the salt from the system. What is to be expected, if the observed nematic phase is really thermodynamically stable, is that the value of the nematic order parameter starts rising to a new equilibrium value. That this is indeed the case is shown in Fig. 3(b). After the time of salt removal the order parameter rises quickly to a value of around 0.7. For much longer simulation time one can expect it to reach the value it has in Fig. 3(a) of about 0.8. This gives strong evidence for a thermodynamically stable nematic phase. Of course, in or-
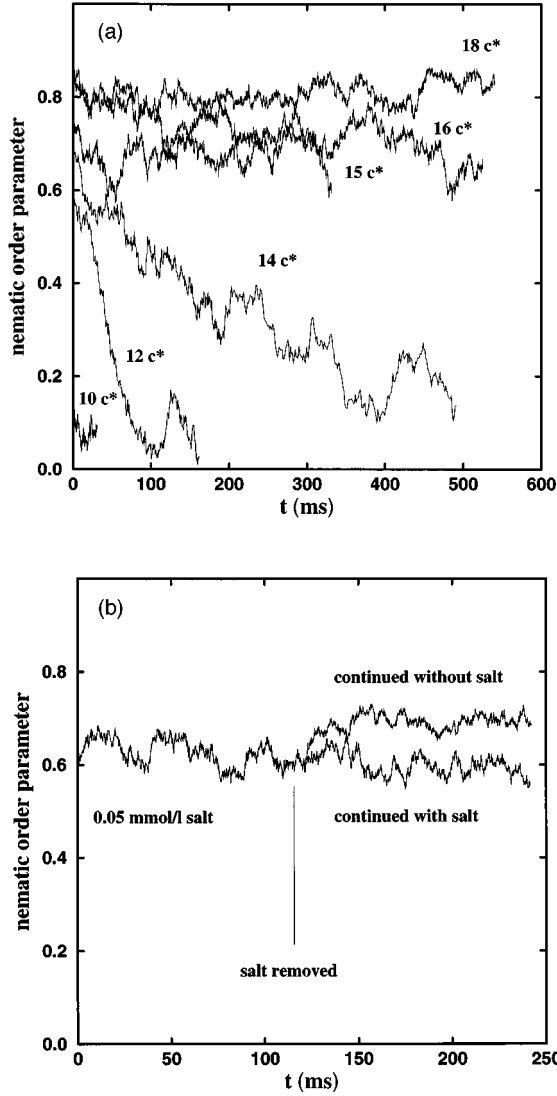
FIG. 3. (a) Nematic order parameter vs time for a salt-free TMV system for different densities. (b) Nematic order parameter vs time for $c = 18c^*$ and a salt concentration of 0.05 mmol/l. At $t = 120$ ms the salt is removed.

der to ensure the global stability of the nematic phase a full thermodynamic calculation has still to be performed.

B. Dynamical correlations

Before presenting explicit results for dynamical correlation functions, we will perform two consistency checks of the program. First, in Fig. 4, $D_{eff}(k)$ is shown for an uncharged TMV suspension ($Q = 0$). The points correspond to BD data, whereas the solid line is obtained from the exact expression of Eqs. (50) and (52). For low values of kL, the statistical error is largely due to the finite simulation box. In the intermediate-k range the agreement is excellent. For $kL \gtrsim 18$ the simulation data systematically fall somewhat below the exact values. This is not due to a principal deficiency but to the numerical evaluation: $S(k,t)$ drops as $\exp(-k^2 D_0 t)$ and the slope of $\ln S(k,t)$ at $t = 0$ has been obtained as $1/S(k)[S(k,\Delta t) - S(k)]/\Delta t$, which is only a very crude estimate of the first time derivative. It would be better
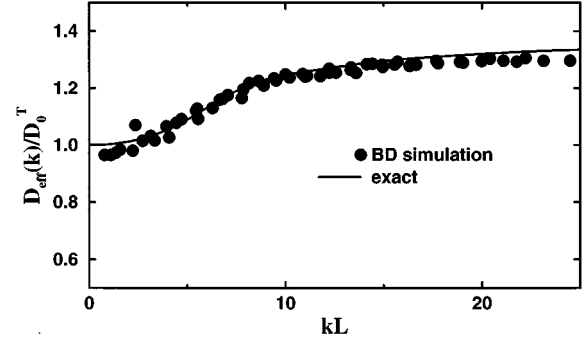

FIG. 4. $D_{eff}(k)$ for a system of noninteracting rods. ● are BD simulation data, and the solid line corresponds to the analytical expression of Eq. (52).

to fit some higher-order polynomial to the first few data points of $S(k,t)$ and to obtain the derivative from it.

The second check of the program is shown in Fig. 5. Here we calculate the static structure factor $S(k)$ both from static and dynamical data according to Eq. (51) for interacting rods. The agreement is quite good, except for high-k values ($kL \gtrsim 50$), where the same explanation as in Fig. 4 applies. For the sake of completeness, also $D_{eff}(k)$ is shown for an interacting system with $Q = 300e$ in Fig. 6. $D_{eff}(k)$ is mainly dominated by the reciprocal of the static structure factor and thus approaches the $D_{eff}(k)$ of the noninteracting system for high-kL values, since $S(k \rightarrow \infty) = 1$. For small-$kL$ values $D_{eff}(k)$ shows a strong increase, since for small k, $S(k)$ is a very small quantity. This increase of $D_{eff}(k)$ with decreasing kL is in qualitative agreement with [21], where an expression is derived for $D_{eff}(k)$ [Eqs. (50)–(52)] using a mean-field ansatz.

We now turn to self-properties as given by the expressions for $W^T(t)$, $W^\perp(t)$, $W^\parallel(t)$, and $W_\angle(t)$. In Fig. 7 results are shown for $W^T(t)$, $W^\perp(t)$, and $W^\parallel(t)$ at three densities ($0.5c^*$, $8c^*$, and $18c^*$).

For low concentration ($c = 0.5c^*$) it takes about $t_0 = 5$ ms, after which the slopes of all three curves coincide. This is due to the aforementioned effect of rotation-translation coupling. Because of the Brownian rotational motion the rod
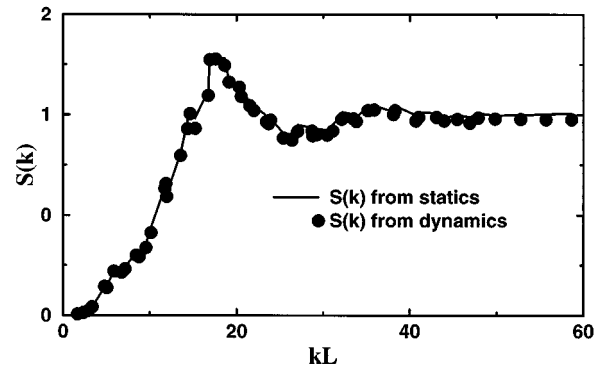

FIG. 5. Static structure factor obtained directly from its definition (solid line) and from the first cumulant of the dynamical structure factor (●). Parameters: $Q = 300e$ and $c = 5c^*$. The other parameters are as in Fig. 1.
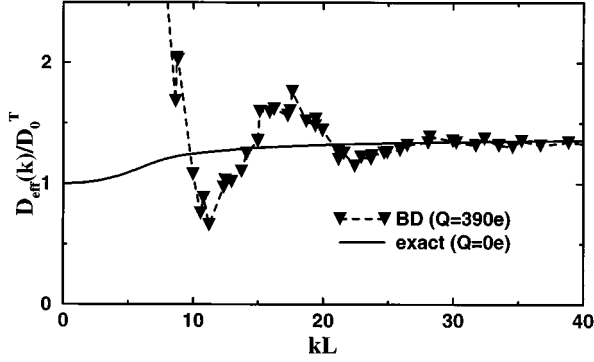
FIG. 6. $D_{\text{eff}}(k)$ for an interacting system ($\bullet$). The lines are a guide to the eye. The single solid line again shows the analytical expression Eq. (52) for $D_{\text{eff}}(k)$ in the noninteracting case.

orientation is completely decorrelated to its initial orientation after t_0. For high concentration ($8c^*$), rotational diffusion slows down strongly due to entanglement effects. Hence the slopes of the three mean square displacement functions become equal only after the significantly larger time of about $t_0 = 25$ ms. At $c = 18c^*$, which is well above the isotropic-nematic phase transition, the behavior of the three mean square displacement functions is quite different from that at concentrations below the critical concentration. Since the rod orientation at time t is always strongly correlated to its initial orientation at time t_0, the slopes of the three mean square displacement functions do not coincide after any time as in parts (a) and (b), but will remain different. Thus it is possible to define long-time translational diffusion coefficients parallel and perpendicular to the rod axis.

Figure 8 shows the ratio of short-time and long-time translational self-diffusion coefficients D_L^T/D_0^T, as obtained by calculating the long-time slope of the mean square displacement $W^T(t)$ versus concentration c over a broad range of densities $c = 0.01 - 24c^*$. First the salt-free case was investigated (black circles). Here it turns out that $D_L^T(c)$ is *nonmonotonic* in c. This can be understood qualitatively by the fact that the strength of the interaction is also density dependent since the density-dependent Debye-Hückel screening length κ enters. This effect also occurs for suspensions of spherical particles interacting via the DLVO potential. Second, when a sufficient amount of single-valenced salt (0.05 mmol/l) is added so that κ is nearly constant with varying c, D_L^T/D_0^T is monotonically decreasing with increasing concentration (full squares in Fig. 8). The increase of D_L^T/D_0^T with added salt with respect to the salt-free case is also known from suspensions of spherical particles [37]. For the density approaching its critical value where the system undergoes the isotropic-nematic phase transition the translational diffusion increases slightly and then stays constant between $16c^*$ and $24c^*$. This can be explained by the fact that topological contraints for the translational movement of the rods are relaxed once they are all approximately parallel. Here we note that the concentration regime explored in this study is significantly larger than that previously investigated by MC studies [11,21], where the maximum concentration was $5.6c^*$.
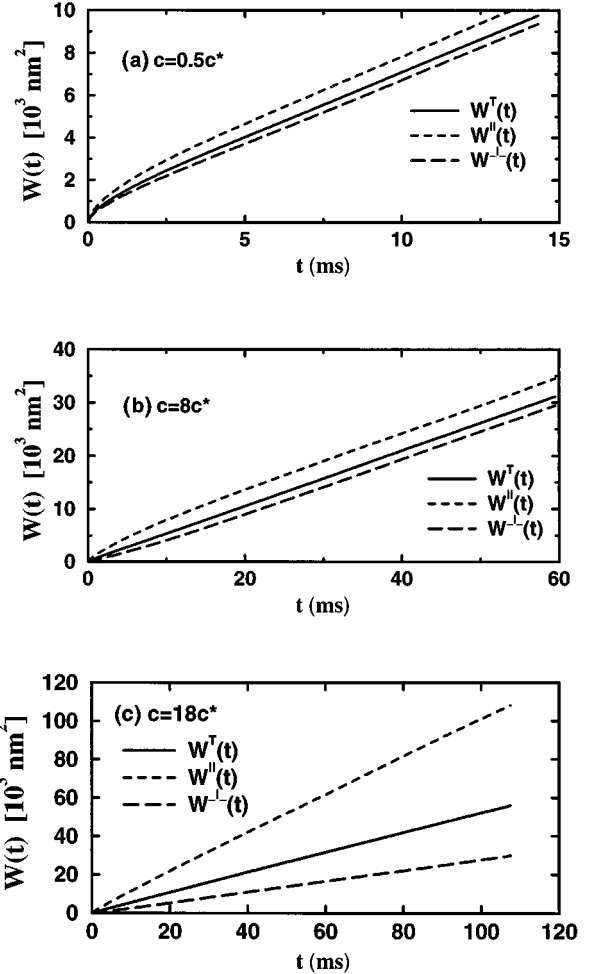

FIG. 7. Mean-square displacements $W^T(t)$, $W^{\perp}(t)$, and $W^{\parallel}(t)$ [see Eqs. (37)] versus time t for three different densities. Units on the Y axis are 10^3 nm^2. (a) $c = 0.5c^*$, (b) $c = 8c^*$, and (c) $c = 18c^*$. For runs (a) and (b) we have chosen $N = 512$ rods and $n = 5$ segments; for run (c) $n = 9$ segments. The other parameters are as in Fig. 1.

The rotational autocorrelation functions $W_{\ell}(t)$ are shown in Fig. 9(a) for $\ell = 1, 2, 3$ and $c = 0.5c^*$. We have plotted $[2/\ell(\ell+1)]\ln W_{\ell}(t)$ versus time. For comparison the data for a free particle are shown as the dash-dotted line. By examining the data carefully, one can distinguish between three time regimes. For extremely short times ($t \ll \tau_0^R$) the rods rotate essentially freely. Because of the growing influence of the interaction with increasing time, the curves start to bend at a time of about 0.05 ms. Until about $\tau_0^R \sim 1.5$ ms all three $W_{\ell}(t)$ curves lie on top of each other. This implies that, on this time scale, the motion practically corresponds to standard diffusion on the unit sphere. However, for longer times ($t \gtrsim \tau_0^R$), the $W_{\ell}(t)$ curves start to deviate from each other. At long times ($t \gg \tau_0^R$) they clearly exhibit different slopes. For $\ell = 1, 2$ a linear fit to the data at these long times is possible, implying an exponential decay of orientational correlations. For $\ell = 3$ the statistical error is too high to extract a unique linear slope, but the curve certainly deviates significantly from the results for $\ell = 1, 2$. Hence the long-
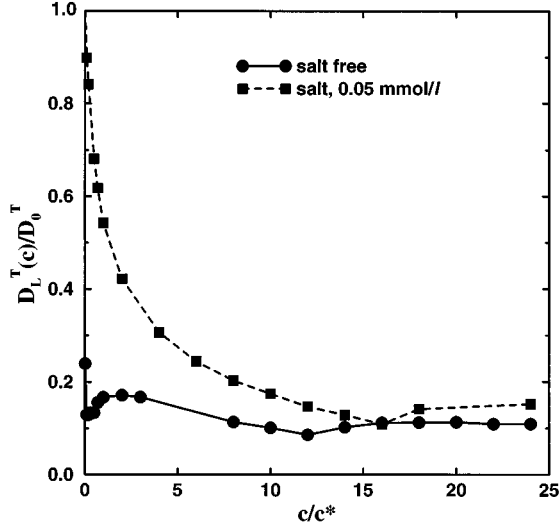
FIG. 8. Long-time translational diffusion coefficient D_L^T measured in terms of its short-time limit D_L^T versus concentration c. Black squares (■) are for a salt-free system, while black circles (●) correspond to a system with a high added monovalent salt concentration of 0.05 mmol/l. The lines are a guide to the eye. The other parameters are as in Fig. 7.

FIG. 9. Orientational correlation functions $W_\ell(t)(\ell=1,2,3)$ [Eq. (47)] for the same parameters as in Fig. 7. (c) $c=18c^*$. We plotted $[2/\ell(\ell+1)]\ln W_\ell(t)$ versus time t measured in units of ms. The dash-dotted line corresponds to the case of a freely diffusing rod.

time orientational self-diffusion coefficient is ℓ dependent. As explained in Sec. V C, the orientational relaxation is therefore not diffusive, i.e., it is not described by the Debye equation on the unit sphere. The same conclusion applies for Fig. 9(b), where $W_\ell(t)$ data for $c=8c^*$ are shown. In this case, due to the strong interaction, the splitting of the three $W_\ell(t)$ curves occurs much later. We have also performed the calculations for very low $(0.01c^*)$ and intermediate concentrations. Qualitatively, we found the same behavior. For $c=0.01c^*$ this is surprising, since one would expect the system to behave essentially gaslike. To verify that this is not the case requires an extreme amount of CPU time, since the correlation functions decay very quickly at this concentration and in order to get any statistical accuracy one needs quite a long trajectory along which to sample. At concentrations above the critical concentration of around $15c^*$ the behavior of the rotational correlation functions changes again. In Fig. 9(c) the concentration is $18c^*$. At time $t=60$ ms the slope for $\ell=2,3$ appears to saturate. The slope is zero within the limit of statistical accuracy. The slope of the $\ell=1$ curve has not yet saturated, which might be due to the separation of time scales among different values of ℓ. Due to finite CPU time resources we could not go to significantly longer measurement times to validate the expected saturation of the $\ell=1$ curve. However, it seems reasonable that the rotational diffusion constant vanishes in a nematic phase. We hence reach the important conclusion that *the orientational relaxation is not diffusive for long times.* This statement is true for the isotropic phase with densities ranging from very dilute $(c=0.01c^*)$ to fairly concentrated $(c=14c^*)$. For densities above the isotropic-nematic transition it is found that there is no true rotational diffusion anymore. For the isotropic phase this point, which was controversially discussed in the literature, needs some further discussion and clarification: There is
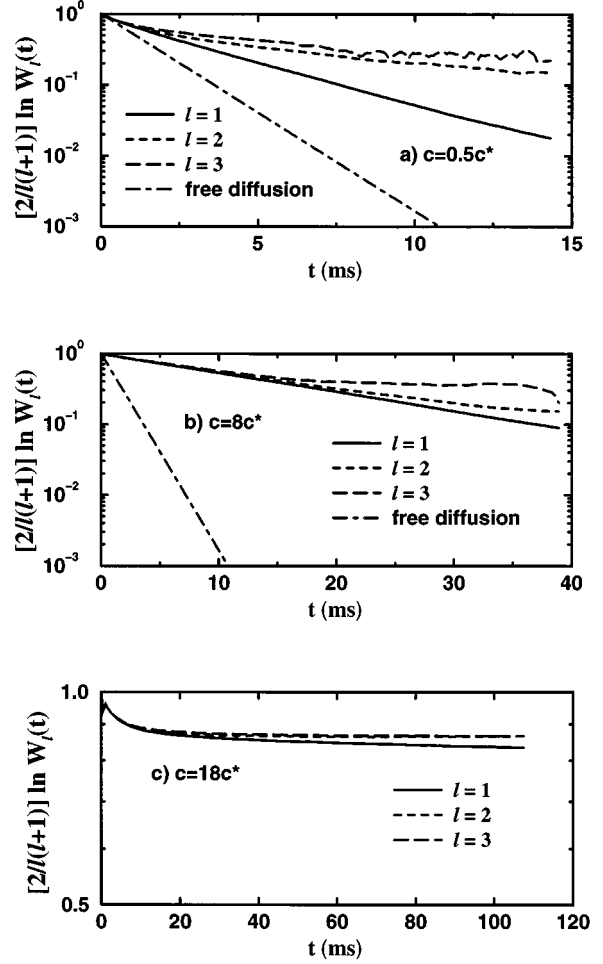
by now general agreement about the behavior of the long-time rotational relaxation, governed by reversible Newtonian dynamics relevant for simple molecular fluids such as H_2O, CS_4 or MeCN. In this case, several authors (see, e.g., [22–24]) have confirmed by simulation that the orientational relaxation is *not* diffusive for long times. For Brownian dynamics, nondiffusivity is in principle conceivable [16], but based on actual BD simulation data it was claimed [14,16] that the long-time orientational motion is diffusive for long times. Our results disagree with this conclusion. Since the nondiffusivity we found occurs on time scales (in units of τ_0^R) that are considerably larger than that explored in the previous BD simulation, we believe that the time scales explored in Refs. [14,16] were not large enough to decide about diffusivity or nondiffusivity.

Long-time orientational motion was also studied for a system of hydrodynamically interacting hard spheres by Jones [38] solving the Smoluchowski equation in an approximate way. He also reached the conclusion that the long-time behavior of the rotational motion is nondiffusive. Although his system is different from ours, the fundamental reason for the
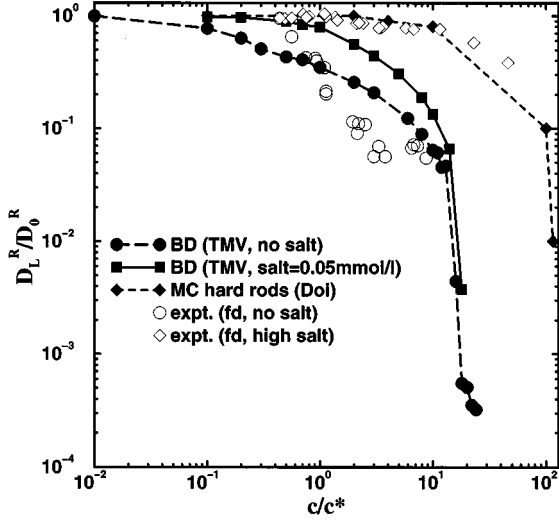
FIG. 10. Long-time orientational diffusion coefficient $D_L^R := \lim_{t \to \infty} D_\ell^R(t)$ for $\ell \equiv 1$ in terms of its short-time limit D_0^R versus concentration c on a double logarithmic scale. ■, BD simulation $D_{\ell=1,L}^R/D_0^R$ with 0.05 mmol/l added salt. ●, same as ■, but in salt-free solution. The other BD parameters are as in Fig. 7. ◆, MC simulation by Doi *et al.* [14]; ◇, experiments with fd virus solutions by Kramer [40] with a completely screened Coulomb interaction by the addition of salt; ○, experiments with fd virus (same as ◇, but under conditions of minimal ionic strength.

nondiffusive character of rotational motion in both systems is really the compactness of the unit sphere on which the rotational degree of freedom moves. To construct a random walk with uncorrelated jumps at long times one ends up with rather large angular displacements, which are not small on any scale with respect to π. Therefore a description in terms of one modified rotational diffusion coefficient is not possible.

We finally remark that it is difficult to see nondiffusive behavior in a birefringence experiment since one only measures D_ℓ^R for fixed $\ell \equiv 2$ and cannot compare with results for other ℓ's. Moreover, it would be necessary to have data for an extended time regime, considerably larger than τ_0^R, to detect nondiffusive behavior.

Finally, in Fig. 10 we show the long-time limit $D_L^R := \lim_{t \to \infty} D_\ell^R(t)$ for $\ell \equiv 1$ in terms of its short-time limit D_0^R versus concentration c. The parameters are as in Fig. 8, but the plot is on a double-logarithmic scale. Full circles correspond to a salt-free situation, while the full squares are for a massive added salt concentration of 0.05 mmol/l so that κ is essentially determined by salt. Both data are clearly monotonically decreasing for increasing concentration.

In Fig. 10, we have also included the results of Doi *et al.* [14] for hard rods (full diamonds) and experimental data (open diamonds and open circles) obtained by Kramer *et al.* [39,40] for a suspension of fd viruses. They are based on birefringence decay experiments at minimal ionic strength (no salt, open circles) and for a high concentration of added salt (open diamonds). In the latter case, one may model the interrod interaction solely by excluded volume effects. Indeed the open diamonds agree quite well with the simulation

data of Doi *et al.* [14]. As a general remark, the time window considered in the experiment is too small to see the nondiffusive behavior of the orientational motion. In fact, the rotational correlation functions obtained in the experiment could be fitted well by a single exponential. Hence it is consistent to compare our long-time data for $D_1^R(t)$ to the experimental data for $D_2^R(t)$.

As regards further comparison of the salt-free data with our results there are several caveats. First, we have used TMV parameters and the data are for an fd suspension. One may hope to scale the basic features out by comparing the ratio D_L^R/D_0^R. But the fd virus has some flexibility that was not accounted for at all in our calculations. Second, it is found experimentally [39] that at the concentration of $0.44c^*$ the measured rotational diffusion coefficient was indistinguishable from the free diffusion coefficient D_0^R, whereas the static structure factor was found to have a peak. These observations are not in agreement with the present results. After these remarks it is clear that one can at most expect a qualitative agreement. Indeed the general behavior is similar to our results. However, details differ much from our data: The simulation data decrease slowly from the value $D_L^R/D_0^R \approx 1$ at the lowest concentration, whereas the experimental data decrease abruptly around $1c^*$ and nearly approach a constant value at about $8c^*$. At the critical concentration of $15c^*$ simulation data decrease sharply and the second derivative appears to change sign. But this could be due to the above-mentioned possibility of not using a sufficiently long measurement time for $D_1^R(t)$. At least the point of phase transition can be identified from this plot. Clearly, for a full direct comparison, experimental data of careful birefringence measurements for well-prepared TMV suspensions over a broad range of concentrations are needed.

VII. CONCLUSION

We presented some results of the Brownian dynamics of large anisotropic rodlike particles interacting through a Yukawa segment-segment potential. The system has been simulated over the range of densities from $0.01c^*$ up to $24c^*$. It was found that the translational motion of the center of mass can be described as a diffusion process similar to the case of spherical macroparticles. In contrast to previous results, it was found that the rotational motion of charged rodlike particles is not a diffusive process at long times. However, there is an intermediate time regime where the motion is practically diffusive.

Future studies plan to address the following questions.

(i) We have so far calculated only one transition point from the isotropic towards a nematic phase. However, the full phase diagram of the Yukawa segment model is not known as a function of rod density and added salt concentration. One may use computer simulation methods [41,42] or density-functional methods [43] to get information about it. Further detailed studies should also investigate the dependence of the phase coexistence lines on the number n of segments.

(ii) As already mentioned, more experiments (birefringence, dynamical light scattering) for carefully prepared and

well-characterized suspensions of rigid rodlike particles are needed to get a more comprehensive picture of the relaxation of rod correlations.

(iii) Theoretically, it would be interesting to include flexibility in the model in order to access the fd virus and other ÿsuspensions of charged semiflexible polymers.

(iv) Finally, hydrodynamic interaction should be included. Indeed, most of the dynamical quantities discussed here are sensitive to such generic many-body interactions and it would be interesting to see how the relaxation of the corre-

lation is affected by hydrodynamic interactions for high concentrations.

[1] F. C. Bawden, N. W. Pirie, J. D. Bernal, and I. Fankuchen, Nature **138**, 1051 (1936).

[2] R. Klein, in *Structure and Dynamics of Strongly Interacting Colloids and Supramolecular Aggregates in Solution*, Vol. 369 of *NATO Advanced Study Institute, Series B: Physics*, edited by S. H. Chen, J. S. Huang, and P. Tartaglia (Kluwer, Dordrecht, 1992).

[3] H. N. W. Lekkerkerker, in *Structure and Dynamics of Strongly Interacting Colloids and Supramolecular Aggregates in Solution* (Ref. [2]).

[4] J. Schneider, W. Hess, and R. Klein, J. Phys. A **18**, 1221 (1985).

[5] J. Schneider, W. Hess, and R. Klein, Macromolecules **19**, 1729 (1986).

[6] J. Schneider, D. Karrer, J. K. G. Dhont, and R. Klein, J. Chem. Phys. **87**, 3008 (1987).

[7] H. Löwen, Phys. Rev. Lett. **72**, 424 (1994); J. Chem. Phys. **100**, 6738 (1994).

[8] E. E. Maier, S. F. Schulz, and R. Weber, Macromolecules **21**, 1544 (1988).

[9] S. F. Schulz, E. E. Maier, and R. Weber, J. Chem. Phys. **90**, 7 (1989).

[10] S. F. Schulz, E. E. Maier, R. Krause, M. Hagenbüchle, M. Deggelmann, and R. Weber, J. Chem. Phys. **92**, 7087 (1990).

[11] M. Hagenbüchle, B. Weyerich, M. Deggelmann, C. Graf, R. Krause, E. E. Maier, S. F. Schulz, R. Klein, and R. Weber, Physica A **169**, 29 (1990).

[12] For such a recent comparison, see, e.g., C. Martin, B. Weyerich, J. Biegel, R. Deike, C. Johner, R. Klein, and R. Weber, J. Phys. (France) II **5**, 697 (1995).

[13] S. Fraden, in *Observations, Prediction, and Simulation of Phase Transitions in Complex Fluids*, *NATO Advanced Study Institute, Series B: Physics*, edited by M. Baus, L. F. Rull, and J. P. Ryckaert (Kluwer Academic, Dordrecht, 1995).

[14] M. Doi, I. Yanamoto, and F. Kano, J. Phys. Soc. Jpn. **53**, 3000 (1984).

[15] M. Fixman, Phys. Rev. Lett. **54**, 337 (1985).

[16] I. Bitsanis, H. T. Davies, and M. Tirrell, Macromolecules **21**, 2824 (1988).

[17] I. Bitsanis, H. T. Davies, M. Tirrell, Macromolecules **23**, 1157 (1990).

[18] H. Löwen, Phys. Rev. E **50**, 1232 (1994).

[19] A. C. Branka and D. M. Heyes, Phys. Rev. E **50**, 4810 (1994).

[20] E. Canessa, B. D'Aguanno, B. Weyerich, and R. Klein, Mol. Phys. **73**, 175 (1991).

[21] B. Weyerich, B. D'Aguanno, E. Canessa, and R. Klein, Faraday Discuss. Chem. Soc. **90**, 245 (1990).

[22] R. M. Lynden-Bell and I. R. McDonald, Mol. Phys. **43**, 1429 (1981).

[23] D. J. Tildesley, P. A. Madden, Mol. Phys. **48**, 129 (1983).

[24] R. M. Lynden-Bell, P. A. Madden, D. T. Stott, and R. J. Tough, Mol. Phys. **58**, 193 (1986).

[25] J. K. G. Dhont and R. Klein, Colloid Polym. Sci. **265**, 289 (1987).

[26] H. van Keulen and J. A. M. Smit, J. Colloid Interface Sci. **170**, 134 (1995).

[27] M. Doi and S. F. Edwards, *The Theory of Polymer Dynamics* (Oxford University Press, Oxford, 1986).

[28] M. M. Tirado, J. G. de la Torre, and C. L. Martinez, J. Chem. Phys. **81**, 2047 (1984).

[29] D. L. Ermak, J. Chem. Phys. **62**, 4189 (1975); **64**, 4197 (1975).

[30] A. Iniesta and J. G. de la Torre, J. Chem. Phys. **92**, 2015 (1989).

[31] G. Chirico and J. Langowski, Macromolecules **25**, 769 (1992).

[32] J. Honerkamp, *Stochastische Dynamische Systeme* (VCH-Verlag, Weinheim, 1990).

[33] M. P. Allen and D. J. Tildesley, *Computer Simulation of Liquids* (Oxford University Press, Oxford, 1987).

[34] M. P. Allen, G. T. Evans, D. Frenkel, and B. M. Mulder, Adv. Chem. Phys. **86**, 1 (1993).

[35] B. J. Berne and R. Pecora, *Dynamic Light Scattering* (Wiley, New York, 1976).

[36] P. Debye, *Polar Molecules* (Dover, New York, 1929).

[37] R. Klein, G. Nägele, and M. Medina-Noyola, in *Ordering and Organizing in Ionic Solutions*, edited by N. Ise and I. Sogami (World Scientific, Singapore, 1988), pp. 543–554.

[38] R. B. Jones, Physica A **157**, 752 (1989).

[39] H. Kramer, M. Deggelmann, C. Graf, M. Hagenbüchle, C. Johner, and R. Weber, Macromolecules **25**, 4325 (1992).

[40] H. Kramer, Ph.D. thesis, University Konstanz, 1993 (unpublished).

[41] J. A. C. Veerman and D. Frenkel, Phys. Rev. A **41**, 3237 (1990).

[42] G. V. Paolini, G. Ciccotti, and M. Ferrario, Mol. Phys. **80**, 297 (1993).

[43] A. Ponierwierski and R. Holyst, Phys. Rev. A **41**, 6871 (1990).